Estimating net community production in the Southern Ocean based on atmospheric potential oxygen and satellite ocean color data

C. D. Nevison,[1] R. F. Keeling,[2] M. Kahru,[2] M. Manizza,[2] B. G. Mitchell,[2] and N. Cassar[3,4]

Received 14 January 2011; revised 20 December 2011; accepted 5 January 2012; published 8 March 2012.

[1] The seasonal cycle of atmospheric potential oxygen (APO ~ O_2 + 1.1 CO_2) reflects three seasonally varying ocean processes: 1) thermal in- and outgassing, 2) mixed layer net community production (NCP) and 3) deep water ventilation. Previous studies have isolated the net biological seasonal signal (i.e., the sum of NCP and ventilation), after using air-sea heat flux data to estimate the thermal signal. In this study, we resolve all three components of the APO seasonal cycle using a methodology in which the ventilation signal is estimated based on atmospheric N_2O data, the thermal signal is estimated based on heat flux or atmospheric Ar/N_2 data, and the production signal is inferred as a residual. The isolation of the NCP signal in APO allows for direct comparison to estimates of NCP based on satellite ocean color data, after translating the latter into an atmospheric signal using an atmospheric transport model. When applied to ocean color data using algorithms specially adapted to the Southern Ocean and APO data at three southern monitoring sites, these two independent methods converge on a similar phase and amplitude of the seasonal NCP signal in APO and yield an estimate of annual mean NCP south of 50°S of 0.8–1.2 Pg C/yr, with corresponding annual mean NPP of ~3 Pg C/yr and a mean growing season *f* ratio of ~0.33. These results are supported by ocean biogeochemistry model simulations, in which air-sea O_2 and N_2O fluxes are resolved into component thermal, ventilation and (for O_2) NCP contributions.

Citation: Nevison, C. D., R. F. Keeling, M. Kahru, M. Manizza, B. G. Mitchell, and N. Cassar (2012), Estimating net community production in the Southern Ocean based on atmospheric potential oxygen and satellite ocean color data, *Global Biogeochem. Cycles*, *26*, GB1020, doi:10.1029/2011GB004040.

1. Introduction

[2] Atmospheric potential oxygen (APO) is a unique atmospheric tracer of ocean biogeochemistry that is calculated by combining high precision O_2 and CO_2 data [*Stephens et al.*, 1998]. APO is effectively the concentration of the molar sum of O_2 + 1.1 CO_2 in air. By design, APO is insensitive to exchanges with the land biosphere, which has a nearly fixed stoichiometry of 1.1 mol O_2 produced (consumed) per mole CO_2 consumed (produced) that produces compensating changes in O_2 and CO_2 resulting from terrestrial photosynthesis and respiration. APO is highly sensitive, however, to exchanges across the air-sea interface, because of the contrasting chemistries of CO_2 and O_2 in surface waters. Carbonate chemistry in seawater strongly damps variability in dissolved CO_2 but has no influence on O_2. As a result, the largest contribution to seasonal cycles in APO arises from air-sea exchange of O_2 due to seasonal variations in upper-ocean biological production and ventilation [*Manning and Keeling*, 2006] with little or no compensation from air-sea exchanges of CO_2. A smaller but also substantial contribution to seasonal variations in APO is driven by warming and cooling of surface waters and the associated changes in gas solubility. APO time series are recorded at a growing number of monitoring sites around the world, beginning as far back as the early 1990s [*Keeling and Shertz*, 1992; *Bender et al.*, 2005; *Battle et al.*, 2006; *Tohjima et al.*, 2008].

[3] Satellite ocean color data have been available since the late 1970s and continuously from 1997 and have revolutionized the monitoring of ocean productivity from seasonal to inter-annual time scales. The most basic surface property or "field" derived from ocean color data is the surface chlorophyll-a concentration, estimated as a function of remotely sensed water-leaving radiances. Starting from estimates of ocean color, higher order fields like vertically integrated net primary production (NPP) can also be derived. The derivation of NPP requires further information about

[1]INSTAAR, University of Colorado at Boulder, Boulder, Colorado, USA.
[2]Scripps Institution of Oceanography, University of California, San Diego, La Jolla, California, USA.
[3]Department of Geosciences, Princeton University, Princeton, New Jersey, USA.
[4]Now at Division of Earth and Ocean Sciences, Nicholas School of the Environment, Duke University, Durham, North Carolina, USA.

0886-6236/12/2011GB004040

the vertical distribution of Chl-a over the depth of the euphotic zone, which is not observable from space and typically must be modeled [*Longhurst et al.*, 1995; *Antoine et al.*, 1996; *Behrenfeld and Falkowski*, 1997]. From NPP, even higher order products, such as export production (EP) can be derived. Estimating EP requires additional parameterizations and input variables, such as sea surface temperature [*Eppley and Peterson*, 1979; *Laws et al.*, 2000; *Laws*, 2004; *Dunne et al.*, 2005]. With each step away from water-leaving radiances, in the progression from Chl-a to NPP to EP, increasing uncertainty is introduced. Current satellite-based estimates of NPP differ by up to a factor of two and estimates of EP have even larger uncertainties [*Carr et al.*, 2006; *Friedrichs et al.*, 2009].

[4] Satellite ocean color data and ground-based observations of APO, as discussed above, provide independent information about the oceanic biogeochemical cycles of carbon and oxygen. Seasonal cycles in APO represent the integrated impact of air-sea oxygen fluxes across broad regions and provide a constraint on a combination of surface production and subsurface mixing processes. Ocean color data constrain near-surface biomass and productivity at high spatial resolution with near-simultaneous spatial coverage, but provide little information on subsurface processes. Ocean color data have a relatively large uncertainty, especially higher order products like NPP and EP, while the mean seasonal cycle in APO is measured at high precision [*Carr et al.*, 2006; *Manning and Keeling*, 2006; *Friedrichs et al.*, 2009; *Saba et al.*, 2010]. Due to their complementary strengths, the combination of APO and satellite ocean color data potentially can provide a more comprehensive constraint on ocean biogeochemistry than either alone.

[5] The uncertainties in satellite ocean color data are especially large in the Southern Ocean [*Carr et al.*, 2006], a region that is critical to the regulation of atmospheric CO_2 [*Caldeira and Duffy*, 2000; *Toggweiler et al.*, 2003]. Conventional ocean color retrievals applicable to the rest of the World Ocean may not be appropriate in this region [*Mitchell and Kahru*, 2009] and likely underestimate phytoplankton stock, NPP and EP by at least a factor of two [*Schlitzer*, 2002].

[6] The Southern Ocean historically has been responsible for a substantial fraction of anthropogenic CO_2 uptake [*Khatiwala et al.*, 2009]. Over the past few decades, however, the strengthening and poleward shift in westerly winds may be causing increased upwelling and ventilation of deep waters around Antarctica that are naturally enriched in CO_2. Studies based largely on coarse resolution ocean models suggest these changes may be reducing the net uptake of CO_2 in this important region [*Wetzel et al.*, 2005; *Lovenduski et al.*, 2007; *Le Quéré et al.*, 2008], although these results may need to be refined by taking into account the influence of subgrid-scale eddies [*Hallberg and Gnanadesikan*, 2006].

[7] A quantitative estimate of EP and its counterpart, net community production (NCP), is important for understanding the global carbon and oxygen cycles and the role of the oceanic "biological pump" in sequestering anthropogenic CO_2. We define NCP here as the net amount of organic carbon fixed over the depth of the mixed layer after accounting for grazing and both autotrophic and heterotrophic respiration. We prefer NCP over the related term "new production," which is commonly defined based on nitrogen fluxes, because NCP can be quantified more precisely in terms of carbon. NCP is closely linked to the air-sea flux of O_2 (F_{O2}), since each mole of photosynthetically fixed carbon that persists beyond 2–3 weeks (the time scale of air-sea exchange) leaves a stoichiometric amount of O_2 available for release to the atmosphere [*Keeling et al.*, 1993]. In contrast, the majority of NPP is quickly remineralized in the mixed layer, with no impact on APO. In the extratropical ocean, the release to the atmosphere of O_2 associated with NCP occurs mainly in spring and summer, when NPP is at its peak.

[8] EP is the flux of organic carbon that sinks out of the mixed layer into the deep ocean. This sinking carbon is generally in particulate form associated with large (micro) phytoplankton or zooplankton [*Uitz et al.*, 2010]. In a steady state system, EP more or less balances NCP. We therefore refer here to the ratio of EP/NPP or NCP/NPP interchangeably as the *f* ratio. EP creates a vertical gradient in dissolved organic carbon that allows the ocean to absorb substantially more atmospheric CO_2 than it would in a perfectly mixed ocean [*Gruber and Sarmiento*, 2002]. The exported carbon is sequestered from the atmosphere and subsequently respired in the subsurface ocean, leading to O_2 depletion at depth. This O_2 is replenished by absorption from the atmosphere when the deep waters mix back to the surface in fall and winter, either through the breakdown of the seasonal thermocline or the high latitude outcropping of isopycnals in the main thermocline. Thus, deep ventilation and NCP are distinct processes that are largely separate in time and space but together form the dominant contributions to the seasonal cycles in APO [*Keeling et al.*, 1993, 1998; *Balkanski et al.*, 1999]. Both processes are closely linked to the "biological pump" critical for ocean uptake of atmospheric CO_2.

[9] While a more direct link exists between NCP and F_{O2} than between EP and F_{O2}, ocean observing programs have primarily focused on measuring EP rather than NCP. A number of models exist for estimating EP as a function of NPP, which have been calibrated against in situ measurements and adapted to satellite ocean color algorithms [*Eppley and Peterson*, 1979; *Laws et al.*, 2000; *Laws*, 2004; *Dunne et al.*, 2005]. Satellite-based estimates of EP are highly uncertain, because, among other reasons, ocean color is a near-surface measurement based on surface irradiance that can at best be only loosely tied to the sinking carbon flux at a standard reference depth such as 100 m. In general, the satellite can only see within the optical depth of the mixed layer and cannot resolve processes, such as additional production or consumption, that occur between the base of the mixed layer and 100 m.

[10] Here, we assume that NCP is approximately equal to EP and that F_{O2} is approximately equal to NCP. This series of simplifying assumptions allows us to directly link F_{O2} and EP through a stoichiometric O_2:C ratio. While the assumptions have many possible shortcomings, a full investigation of the relationship between F_{O2} and EP is beyond the scope of this paper. Our simplifying assumptions allow us to skirt the problem of possible phase offsets between F_{O2} and EP [*Balkanski et al.*, 1999], since the timing of F_{O2} is more directly linked to NCP than it is to EP, although small phase delays due to air-sea exchange still might occur.

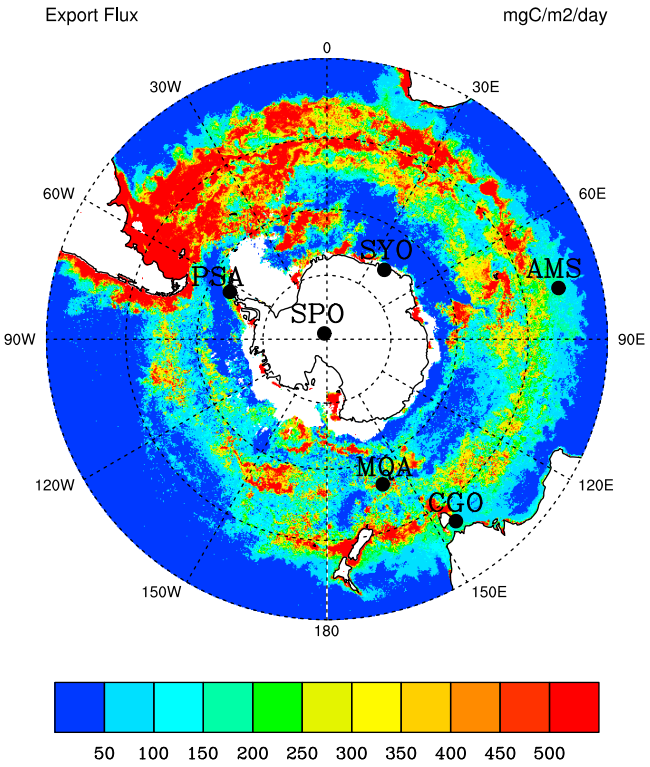

Figure 1. Export production (EP12) in mg C m^{-2} day^{-1} in January from satellite data described in Section 2.3. Locations of six APO monitoring stations are superimposed.

[11] In this paper, we estimate the climatological seasonal cycle in NCP in the Southern Ocean in terms of both integrated oceanic fluxes and their impact on APO. We compare three different methods. First, we estimate NCP based on satellite ocean color data, assuming an equivalence between EP and NCP and the associated air-sea O_2 flux. Second, we use a 3-dimensional ocean biogeochemistry model to estimate the air-sea O_2 flux associated with NCP. Third, we use the mean seasonal cycle in APO data, correcting for the ventilation component using atmospheric N_2O data and correcting for the thermal component using either atmospheric Ar/N_2 or ocean heat flux data [*Keeling et al.*, 2004; *Cassar et al.*, 2008]. This leaves the NCP contribution to the APO cycle as a residual [*Nevison et al.*, 2005]. To allow the three methods to be compared on a common basis, the air sea O_2 fluxes from the first two methods are carried in an atmospheric transport model to estimate the NCP contributions to the APO cycle at atmospheric baseline stations in the Southern Ocean. A primary goal of the study is to explore the use of observed seasonal cycles in APO to quantitatively constrain oceanic carbon and oxygen fluxes derived from satellite ocean color data.

2. Methods

2.1. APO Data

[12] Atmospheric O_2 data, reported in terms of deviations in the O_2/N_2 ratio, were obtained from the Scripps Institution of Oceanography (SIO) and Princeton University (PU) networks (see Text S1 in the auxiliary material for details of the measurement techniques).[1] Data are available from the early to mid 1990s, depending on the station [*Keeling et al.*, 1996; *Bender et al.*, 2005; *Manning and Keeling*, 2006]. There are 6 stations located south of 30°S, which we use to define the "Southern Ocean" region (AMS, CGO, MQA, PSA, SPO, SYO). Details are listed in Table S1 and station locations are shown in Figure 1. The SIO and PU networks have 3 to 4 stations each in the Southern Ocean, including a common station at CGO. In this paper, we define the APO tracer according to,

$$\mathrm{APO} = \delta(\mathrm{O_2/N_2}) + \frac{1.1}{X_{O2}}\mathrm{CO_2}, \quad (1)$$

where $\delta(O_2/N_2)$ is the relative deviation in the O_2/N_2 ratio from a reference ratio in per meg units, X_{O2} = 0.2095 is a the O_2 mole fraction of dry air [*Stephens et al.*, 1998], CO_2 is the mole fraction of carbon dioxide in parts-per million (μmol mol^{-1}), and 1.1 is the average -O_2:C ratio of terrestrial respiration and photosynthesis. Mean seasonal cycles for APO (Figure 2), and for all other atmospheric species both observed and modeled as discussed below, are estimated as the harmonic component of a 3rd order polynomial plus first 4 harmonics fit to each monthly mean time series [*Thoning et al.*, 1989]. At Southern Ocean stations, the seasonal cycles in $\delta(O_2/N_2)$ dominate the cycles in APO because the seasonal cycles in CO_2 are small.

2.2. N_2O and Complementary CFC-12 Data

[13] The details of the N_2O and CFC-12 data used in this study are given in Text S1. An important assumption is that the observed mean seasonal cycle of atmospheric N_2O contains information about the biological ocean source of N_2O, which in turn can be related to the seasonal ventilation signal in APO. Since the amplitude of the observed N_2O cycle is small, i.e., only about 0.2% of the mean tropospheric N_2O mixing ratio, it is debatable whether a mean seasonal cycle in the available N_2O data can be resolved and whether enough information exists about other components of the N_2O seasonal cycle to estimate and subtract them to isolate the oceanic component. These questions have been investigated by *Nevison et al.* [2005, 2011], who conclude that ventilation of microbially enriched deep water in the Southern Ocean contributes to the spring maximum in the N_2O seasonal cycle, but that there is a complicating stratospheric influence on the N_2O seasonal cycle at southern hemisphere stations that is similar in phase to the oceanic source signal and a complicating thermal signal that opposes the oceanic ventilation signal. The thermal signal can be estimated as described in Section 2.5 and Text S1, while the stratospheric signal can be estimated on the basis of the mean seasonal cycle of CFC-12.

2.3. Satellite Ocean Color Data

[14] Net primary production (NPP), export production (EP) and corresponding air-sea O_2 fluxes were estimated based on Chl-a fields derived from satellite ocean color data. The estimates were made globally, but with an emphasis on

[1] Auxiliary materials are available in the HTML. doi:10.1029/2011GB004040.

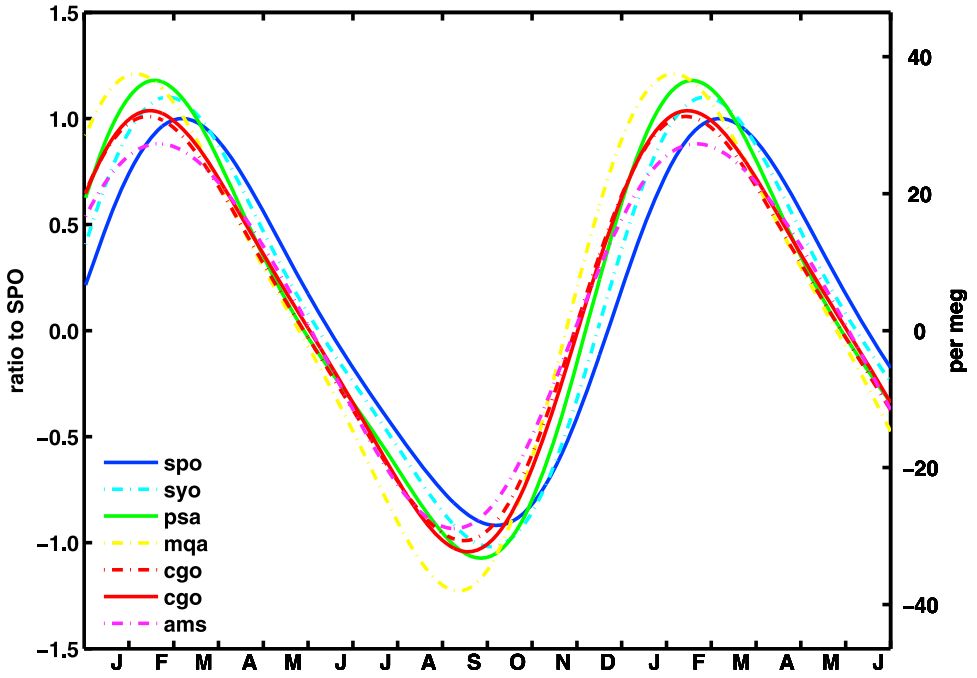

Figure 2. Observed APO mean annual cycles at six Southern Ocean stations. Solid lines are SIO stations. Dashed lines are PU stations. Left axis shows the ratio of the maximum amplitude normalized to the South Pole (SPO) station. Right axis shows absolute value in per meg.

the Southern Ocean, which effectively dominates the APO seasonal cycle at the Southern Hemisphere APO monitoring stations [*Garcia and Keeling*, 2001]. Current standard satellite algorithms under-estimate Chl-a by 2–3 times over the middle range of Chl-a in the Southern Ocean, due to the special bio-optical properties of the region [*Mitchell and Holm-Hansen*, 1991; *Mitchell*, 1992]. This bias is transferred to higher level products like NPP and EP that use Chl-a as input. We used a special empirical algorithm, SPGANT, to estimate Chl-a in the Southern Ocean, which was blended with the standard algorithms for the rest of the world ocean [*Mitchell and Kahru*, 2009; *Kahru and Mitchell*, 2010]. The blended Chl-a was input to a modified version of the VGPM model to calculate NPP [*Behrenfeld and Falkowski*, 1997], with parameters tuned to the Southern Ocean. We calculated export production (EP) based on the *Laws* [2004] model as a function of NPP and SST. Text S1 describes the satellite data and algorithms in more detail.

[15] The integrated fluxes of NPP and EP for the global ocean calculated above were NPP = 55 Pg C/yr and EP = 17 Pg C yr^{-1} (1.4 Pg C yr^{-1} south of 50°S). 50°S is the average position of the wind stress maximum in the Southern Ocean and the waters south of this latitude are characterized by upwelling [*Pollard et al.*, 2006]. The NPP estimate is near the middle of the range of alternate satellite-based estimates (35–70 Pg C yr^{-1}) [*Carr et al.*, 2006], while the EP total is substantially higher than the commonly cited estimate of 11 Pg C yr^{-1} (1 Pg C yr^{-1} south of 50°S) based on the ocean inversion of *Schlitzer* [2002]. The high EP estimate was associated with *f* ratios that frequently exceeded 0.5 in the Southern Ocean (resulting from the propagation of the relatively large SPGANT Chl-a fields through the VGPM and *Laws* models). As a sensitivity study, we calculated an alternate set of EP fluxes by scaling down our standard fluxes by a factor of 0.725 to agree with the *Schlitzer* [2002] value of 1 Pg C yr^{-1} for the Southern Ocean south of 50°S. This second set of fluxes yielded a global EP of 12 Pg C yr^{-1} with an average *f* ratio of 0.33 south of 50°S. Both sets of EP fluxes were converted to air-sea O_2 fluxes F_{O2}, assuming EP ~ NCP ~ F_{O2}, using a stoichiometric -O_2:C ratio of 1.4 mol/mole [*Laws*, 1991; *Anderson*, 1995]. The uncertainty in the -O_2:C ratio is relatively small, with estimates ranging from 1.3 to 1.6 [*Jin et al.*, 2007].

2.4. Ocean Biogeochemistry Model

[16] We used the MIT three-dimensional ocean general circulation model [*Marshall et al.*, 1997a, 1997b] in a coarse resolution global configuration (2.8° × 2.8°, 15 vertical levels) to simulate various components of the air-sea O_2 flux. The physical model is forced by monthly mean climatological data [*Dutkiewicz et al.*, 2005]. The biogeochemistry module is based on pelagic ecosystem dynamics and represents the coupled cycles of phosphorus, silicon, and iron. It explicitly simulates two "functional groups" of phytoplankton, nominally diatoms (microphytoplankton) and small (nanophytoplankton), and one generic zooplankton group. More complete details are given by *Dutkiewicz et al.* [2005] and *Ito et al.* [2005].

[17] We decomposed the modeled air-sea O_2 flux into thermal, deep ventilation and net community production (NCP) terms. The decomposition was achieved by linear combinations of 3 different simulations, all run 2000 years to achieve a steady state mean annual cycle: 1) a normal run with full biology, "Total Oxygen" ($O_{2(tot)}$), 2) a run that unconditionally shuts off all biological activity "Thermal O_2" ($O_{2(th)}$), such that the only processes besides transport and mixing affecting $O_{2(th)}$ are solubility changes due to

seasonally varying heat fluxes at the ocean surface, and 3) a run setting the local production and respiration terms to zero whenever NCP would otherwise be greater than zero, i.e., in the euphotic zone. In addition to transport and mixing, this third species "Aphotic Oxygen" ($O_{2(ap)}$) is affected only by thermal processes and dark respiration occurring in the subsurface ocean. The deep ventilation tracer $O_{2(vent)}$ was estimated as the difference $O_{2(ap)} - O_{2(th)}$. The NCP tracer $O_{2(NCP)}$ was estimated as the difference $O_{2(tot)} - O_{2(ap)}$. The global total NCP predicted with this formulation is 17 Pg C/yr (2 Pg C/yr south of 50°S) using the model's 1.4 mol -O_2:C conversion.

[18] In addition to the O_2 decomposition, two new prognostic chemical species were added to the model: 1) N_2, a tracer with no modeled biological sources or sinks but which responds to thermal solubility changes in the upper ocean, and 2) N_2O, a tracer also responding to thermal solubility changes (assuming a background atmospheric N_2O concentration of 320 ppb) but also with a microbial ocean source parameterized as a simple function of the subsurface O_2 consumption flux with a constant coefficient of 0.122×10^{-3} mole N_2O produced per mole O_2 consumed [*Suntharalingam and Sarmiento*, 2000]. (This parameterization overestimates the observed ΔN_2O/AOU ratio in the Southern Ocean by about a factor of 2 – see Section 2.7). For simplicity and since our focus was the relatively O_2-rich Southern Ocean, we assumed no biological sinks for N_2O. In addition to total N_2O, a prognostic thermal-only species N_2O_{therm} was computed in the MIT model by shutting off the biological source term. N_2O_{bio} was inferred as the difference between N_2O_{tot} and N_2O_{therm}. Since N_2O production in the surface layer was not allowed, due to light inhibition of nitrifying bacteria [*Horrigan et al.*, 1981], N_2O_{bio} was essentially a tracer of deep ventilation, i.e., $N_2O_{vent} \sim N_2O_{bio}$.

2.5. Thermal Fluxes

[19] The seasonal cycle of atmospheric O_2/N_2 due to thermal in/outgassing was estimated using two approaches. First, the thermal signal in atmospheric O_2/N_2 was estimated based on measurements of changes in the atmospheric Ar/N_2 ratio, which is reported similarly to O_2/N_2 data in per meg units. The atmospheric Ar/N_2 ratio varies seasonally because of thermal ingassing and outgassing of both Ar and N_2. Ar has a higher solubility and solubility-temperature dependence than N_2, leading to larger relative changes in atmospheric Ar than N_2. The biological influences on the Ar and N_2 exchanges are both negligible. Ar/N_2 is monitored at the same stations as O_2/N_2 by long-term flask sampling programs maintained by PU and SIO [*Battle et al.*, 2003; *Keeling et al.*, 2004; *Cassar et al.*, 2008]. The small changes in Ar/N_2 relative to a large background are difficult to measure precisely, but the time series span nearly a decade or more at all sites, permitting the calculation of the mean seasonal cycle $(Ar/N_2)_{seas}$ using the polynomial and harmonic fit described in Section 2.1. The seasonal cycles in O_2/N_2, N_2O and CFC-12 due to thermal effects are estimated based on $(Ar/N_2)_{seas}$ using scaling factors derived from the ratios of the temperature derivatives of the respective solubility functions (see Text S1). We refer to these as $(O_2/N_2)_{therm,Ar}$, $N_2O_{therm,Ar}$ and CFC-$12_{therm,Ar}$.

[20] Second, surface fluxes F of O_2 and N_2 were estimated as $F = QS_T/C_p$ [*Keeling et al.*, 1998], where Q is the NCEP heat flux [*Kalnay et al.*, 1996], S_T is the temperature derivative of O_2 or N_2 solubility evaluated at the NCEP sea surface temperature and C_p is the heat capacity of seawater. (Thermal fluxes of N_2 influence O_2/N_2 via a dilution effect and therefore must be included in the heat flux-based calculations.) In addition, a modified flux was calculated as by *Jin et al.* [2007], who optimized the formula based on comparisons to prognostic thermal O_2 fluxes from an ocean model. For the modified flux, the magnitude of F was scaled down by a factor of 1/1.3 and the flux was delayed for half a month. We assumed that these same modifications were valid for the N_2 fluxes. Both sets of O_2 and N_2 fluxes were used to force the MATCH atmospheric transport model and converted into an atmospheric signal in per meg units (see Section 2.6).

2.6. Atmospheric Transport Model

[21] We used the Model of Atmospheric Transport and Chemistry (MATCH) [*Rasch et al.*, 1997; *Mahowald et al.*, 1997] to translate surface air-sea fluxes into corresponding atmospheric signals. MATCH was run at T62 horizontal resolution (about 1.9° latitude by longitude) with 28 vertical levels and a time step of 20 min using archived 6 hourly winds for the years 2000–2003 from the National Center for Environmental Prediction (NCEP) reanalyses [*Kalnay et al.*, 1996]. The model was forced with a variety of surface fluxes, including the air-sea O_2 fluxes associated with the satellite-based NCP described in Section 2.3, the MIT ocean model air-sea O_2 and N_2 fluxes described in Section 2.4, and the thermal O_2 and N_2 fluxes described in Section 2.5. The resulting MATCH tracers were used to compute the APO signals due to thermal process, net community production, and ventilation using equations (2), (3), and (4), respectively. Total APO for the MIT model was calculated with equation (5).

$$\text{ATM-THERM}_{\text{i}} = \frac{1}{X_{o2}} O_{2,therm} - \frac{1}{X_{N2}} N_2, \text{i} = \text{Q or Qmod} \quad (2)$$

$$\text{ATM-NCP}_{\text{j}} = \frac{1}{X_{o2}} O_{2,NCP}, \text{j} = \text{EP12, EP17 or MIT} \quad (3)$$

$$\text{ATM-VENT}_{\text{MIT}} = \frac{1}{X_{o2}} \text{O}_{2,\text{vent}}, \quad (4)$$

$$\text{ATM-APO}_{\text{MIT}} = \frac{1}{X_{O2}} O_{2,total} - \frac{1}{X_{N2}} N_2, \quad (5)$$

where X_{O2} and X_{N2} are the reference mole fractions of O_2 and N_2 in air (0.2095 and 0.7808, respectively), the subscripts Q and Qmod for ATM-THERM distinguish heat flux-based calculations with and without *Jin et al.*'s [2007] modifications (Section 2.5), the subscripts EP12 and EP17 for ATM-NCP refer to the global integrals of satellite-based EP in Pg C yr^{-1} (Section 2.3) and all MIT subscripts refer to values from the ocean biogeochemistry model (Section 2.4) Strictly speaking, the products of equations (2)–(5) represent O_2/N_2 rather than APO (see equation (1)), since there are small oceanic CO_2 fluxes associated with thermal ingassing and outgassing, NCP and ventilation. However, we assume

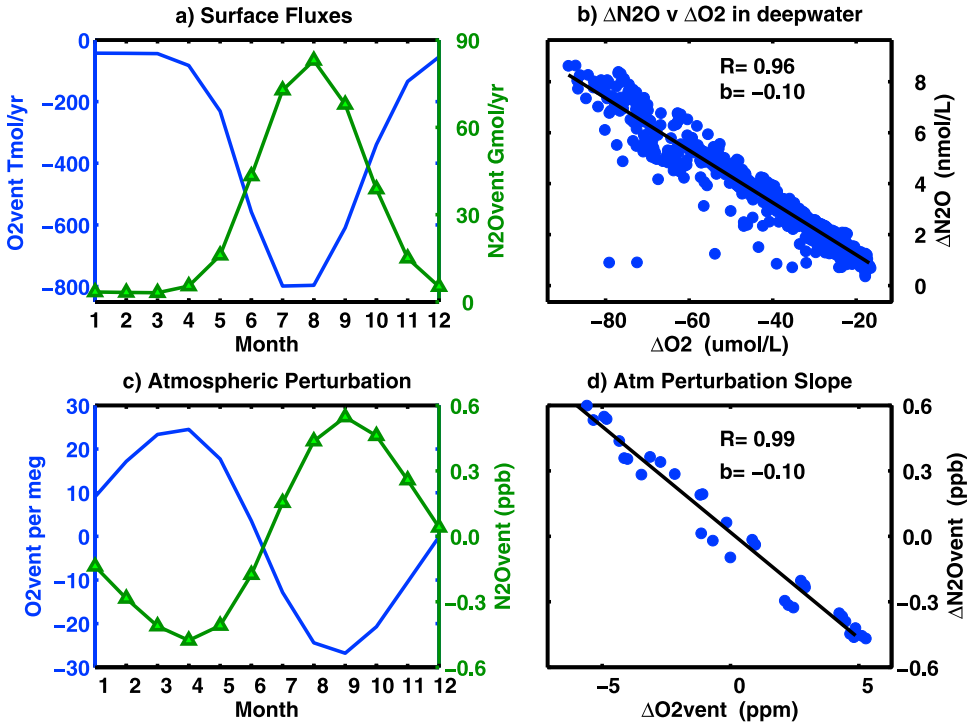

Figure 3. Results of (top) MIT ocean model and (bottom) corresponding MATCH simulation, illustrating the basis for the N_2O method for estimating APO_{vent}. (a) Air-sea fluxes of $O2_{vent}$ and $N2O_{vent}$ integrated from 45 to 60°S. (b) ΔN_2O (= N_2O-N_2O_{sat}) versus ΔO_2 (= O_2-$O_{2,sat}$) ratio at 85 m in July in MIT ocean model, showing all values from 45 to 60°S. (c) Mean atmospheric seasonal cycle of ATM-$VENT_{MIT}$ and ATM-N_2OVENT_{MIT}. (d) Slope of detrended monthly mean results for ATM-$VENT_{MIT}$ versus ATM-N_2OVENT_{MIT} over 3 model years.

that these oceanic CO_2 terms make a relatively small contribution to the mean seasonal cycle in APO compared to the uncertainties in the O_2 terms themselves. We make a similar assumption that $(O_2/N_2)_{therm,Ar} \sim APO_{therm,Ar}$ for the argon-based thermal signal discussed in Section 2.5. These assumptions may not be valid in the tropics, where strong oceanic CO_2 outgassing occurs and O_2 fluxes are not strongly seasonal, but are reasonable for the Southern Ocean [*Nevison et al.*, 2008].

[22] Additional MATCH simulations were performed with the biological air-sea fluxes of N_2O, both from the MIT model as described above and from the 3-dimensional ocean biogeochemistry model of *Jin and Gruber* [2003]. These simulations yielded atmospheric N_2O tracers referred to here as ATM-N_2OVENT_{MIT} and ATM-N_2OVENT_{JG}. Similarly, thermal N_2O tracers ATM-$N_2OTHERM_Q$ and ATM-$N_2OTHERM_{Qmod}$ were estimated by forcing MATCH with thermal N_2O fluxes estimated based on the $F = QS_T/C_p$ equation, with and without the *Jin et al.* [2007] modifications, where S_T is the temperature derivative of the N_2O solubility coefficient [*Weiss and Price*, 1980].

2.7. Decomposition of Observed APO Seasonal Cycle

[23] Equation (6a) and (6b) describe the component signals of the observed mean seasonal cycle in APO.

$$APO_{obs} = APO_{therm} + APO_{netbio} \quad (6a)$$

$$= APO_{therm} + APO_{vent} + APO_{NCP} \quad (6b)$$

A number of studies have estimated APO_{therm} using equation (2) and then rearranged equation (6a) to isolate the net biological seasonal cycle APO_{netbio} [*Stephens et al.*, 1998; *Keeling et al.*, 1998; *Balkanski et al.*, 1999; *Najjar and Keeling*, 2000; *Garcia and Keeling*, 2001]. While APO_{netbio} can be indirectly related to NCP via concepts like Seasonal Net Outgassing (SNO), it cannot be compared directly to satellite ocean color data, since the latter provide no information about deep ventilation. This problem has complicated past efforts to quantify NCP based on the seasonal amplitude of APO_{netbio} [*Keeling and Shertz*, 1992; *Bender et al.*, 1996; *Najjar and Keeling*, 2000]. Here, we partition APO_{netbio} into ventilation and production components (equation (6b)), which in principle can be compared directly to the ATM-VENT and ATM-NCP tracers described above and thus related quantitatively to the underlying air-sea fluxes.

[24] Our approach, first described in *Nevison et al.* [2005], uses the observed seasonal cycle in atmospheric N_2O and the close correlation between N_2O production and O_2 consumption in the subsurface ocean [*Yoshinari*, 1976; *Cohen and Gordon*, 1978; *Butler et al.*, 1989] to estimate the ventilation signal in APO. This allows the production term APO_{NCP} to be inferred as a residual,

$$APO_{NCP} = APO_{obs} - APO_{therm} - APO_{vent}, \quad (7)$$

$$\text{where } APO_{vent} = -\frac{1}{\left(\frac{\Delta N_2O}{AOU}\right)} N_2O_{vent} \quad (8)$$

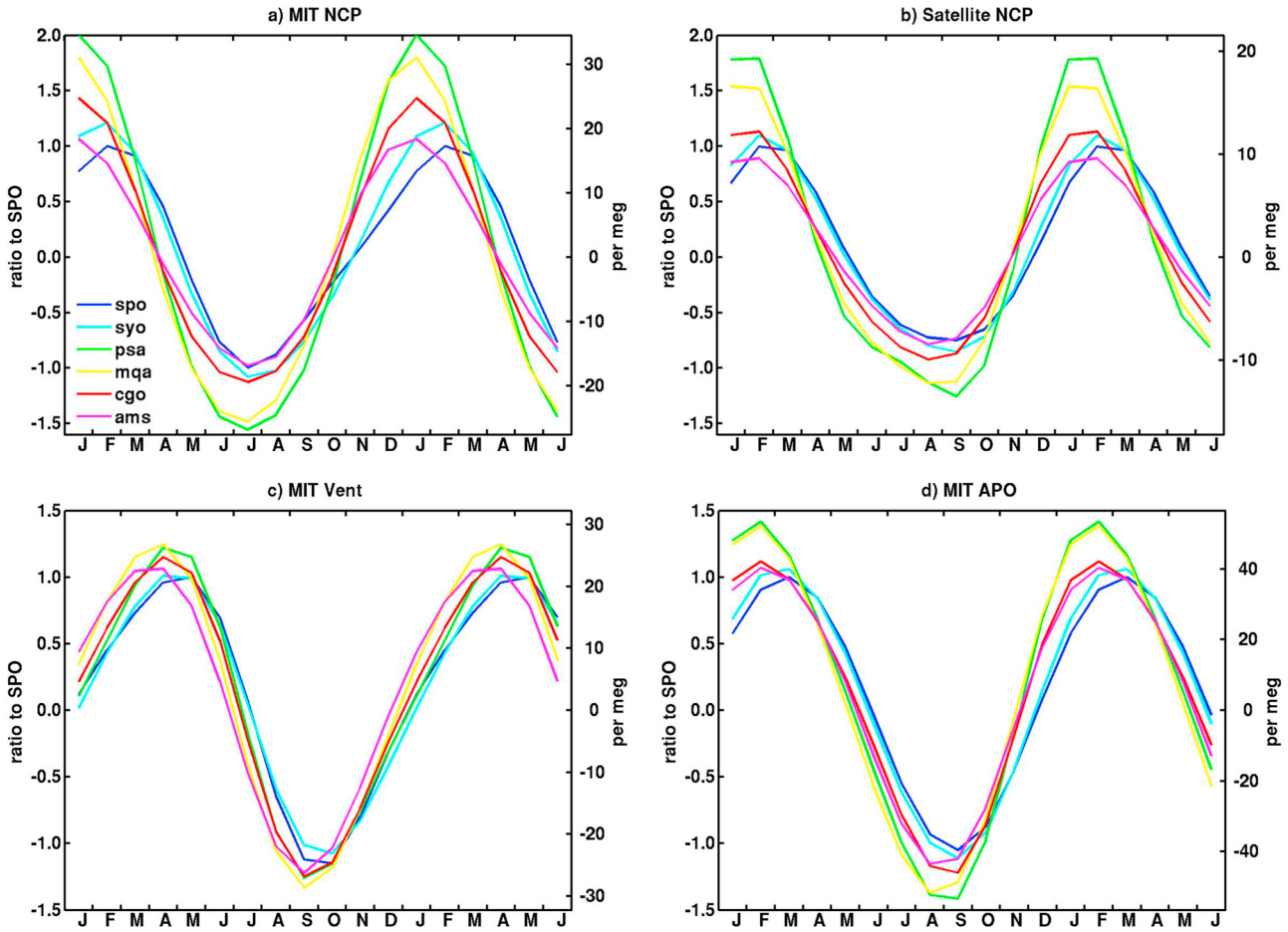

Figure 4. Comparison at six Southern Hemisphere monitoring sites of modeled mean seasonal cycles in total APO or its components, as derived from MATCH simulations forced by air-sea fluxes from the MIT ocean model or satellite ocean color data: (a) ATM-NCP_{MIT}, (b) ATM-NCP_{EP12} (i.e., satellite-derived NCP with global total of 12 PgC/yr), (c) ATM-$VENT_{MIT}$, (d) ATM-APO_{MIT}. See Sections 2.3, 2.4, and 2.6 for details.

Equation (8) assumes that APO_{vent} can be related to N_2O_{vent} by dividing by the subsurface $\Delta N_2O/AOU$ ratio (an approximate measure of the rate of N_2O production to O_2 consumption). This assumption was inspired by observations at a California coastal upwelling site [*Lueker et al.*, 2003] and is supported by our MATCH:MIT simulations (Figure 3). The $\Delta N_2O/AOU$ ratio is relatively well known in the Southern Ocean based on observed N_2O and O_2 depth profiles [*Nevison et al.*, 2003; 2005]. We assume a value of 0.05×10^{-3} mole/mole with a range of uncertainty of $\pm 0.01 \times 10^{-3}$.

[25] N_2O_{vent} was estimated based on the observed mean seasonal cycle of atmospheric N_2O, after estimating and subtracting off thermal (N_2O_{therm}) and stratospheric/remote components (N_2O_{strat}). We estimated N_2O_{therm} based either on heat flux or Ar/N_2 data, as described in Section 2.5. We estimated N_2O_{strat} based on the observed mean seasonal cycle of CFC-12, a relatively insoluble gas with a similar lifetime and stratospheric sink as N_2O. Text S1 provides the details of the estimation of N_2O_{vent}.

[26] Tables S2 and S3 in the auxiliary material list the various terms in the decomposed seasonal cycles of APO and N_2O, respectively. Our nomenclature makes a primary distinction between terms that are derived directly from atmospheric data, versus those estimated using the MATCH atmospheric transport model (terms beginning with ATM). However, we note that some terms like APO_{NCP} and N_2O_{vent}, which are calculated as residuals, in some cases may be derived from a combination of direct atmospheric data and thermal tracers simulated by the MATCH model. In addition, we use the unqualified terms APO_{therm} and N_2O_{therm} generically to refer to either Ar/N_2 or heat flux-based thermal signals.

3. Results

3.1. Patterns Across Southern Ocean Monitoring Sites

[27] APO data are available from six stations south of 30°S in the Southern Ocean (Table S1 in the auxiliary material). Of these, three (CGO, MQA, PSA) are situated close to the most biologically productive regions (Figure 1), one (AMS) lies somewhat equatorward, and two (SYO and SPO) sit on the Antarctic continent, separated by land or ice from the most productive regions. The amplitudes at MQA and PSA are about ~20% larger than those at the other stations and there is a trend toward later maxima as one

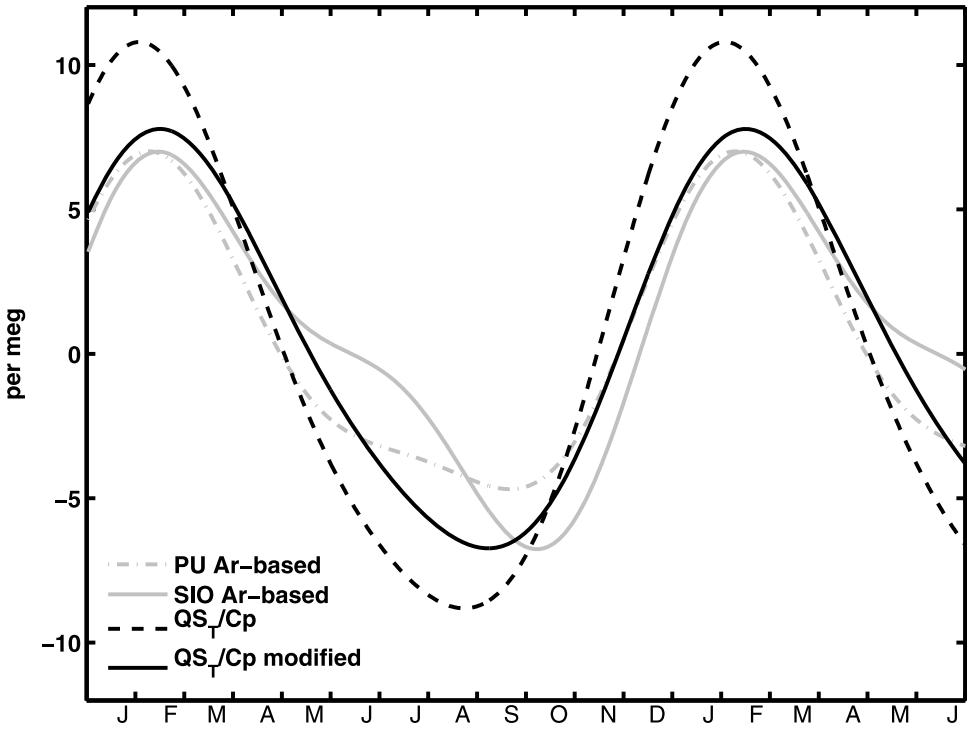

Figure 5. Thermal APO signal at CGO. Two of the signals are modeled based on ocean heat fluxes run in the MATCH atmospheric transport model. Two of the signals are based on Ar/N_2 data. See Section 2.5 for details.

moves poleward (Figure 2). The ATM-NCP tracers show similar trends in phasing relative to observations but a stronger differentiation in amplitude, with peak-to-trough values at MQA and PSA some 50–80% larger (for satellite-based ATM-NCP_{EP12}) and 80–100% larger (for ATM-NCP_{MIT}) than those of the other stations (Figures 4a and 4b). The ATM-$VENT_{MIT}$ and, consequently, the total ATM-APO_{MIT} tracers show considerably smaller differentiation in amplitude across the six stations (Figures 4c and 4d).

3.2. Thermal APO Signal

[28] The decomposition of the observed APO seasonal cycle begins with an estimate of the thermal contribution, APO_{therm}, which can be subtracted from the observed cycle to estimate the net biological signal (equation (6a)). Four different estimates of APO_{therm} at station CGO, two based on observed Ar/N_2, two modeled based on the QS_T/Cp formula (see Section 2.5), are compared in Figure 5, showing relatively good agreement in phase. The maxima range from late January to mid February. The spread in minima is somewhat larger, ranging from August for ATM-$THERM_Q$ to October for SIO $APO_{therm,Ar}$. With respect to seasonal amplitude, the ATM-$THERM_Q$ cycle appears as an outlier that is nearly 50% larger than the mean of the other three.

[29] As shown in Figure 5, the *Jin et al.* [2007] modifications to QS_T/Cp cause the modeled thermal signal, ATM-$THERM_{Qmod}$, to agree better with $APO_{therm,Ar}$, both with respect to phase and amplitude. Past studies generally have used the unmodified QS_T/Cp formula to estimate the thermal APO cycle [*Stephens et al.*, 1998; *Keeling et al.*, 1998; *Najjar and Keeling*, 2000; *Garcia and Keeling*, 2001]. While the Jin *et al.* approach seems physically sound, at present it cannot be definitively tested using Ar/N_2 data because of large uncertainties in both the Ar/N_2 data [*Cassar et al.*, 2008] and the transport models needed to translate air-sea O_2 and N_2 fluxes into ATM-THERM signals [*Blaine*, 2005; *Naegler et al.*, 2007]. In contrast, the conversion of Ar/N_2 into a thermal O_2/N_2 signal using scaling factors based on the respective Ar and O_2 solubility functions is a minor uncertainty (M. Manizza et al., Resolving the seasonal components of air-sea gas fluxes in the global ocean: A modeling study, manuscript in preparation, 2012).

[30] Several studies have compared Ar/N_2 data directly to ATM simulations forced with air-sea Ar and N_2 fluxes. The latter have been estimated both diagnostically with the (unmodified) QS_T/Cp equation, and prognostically in the context of 3-dimensional ocean models that account for phase lags and incomplete thermal equilibration [*Battle et al.*, 2003; *Cassar et al.*, 2008]. The results have varied by monitoring site and thus have defied a one-size-fits-all interpretation. At CGO, both the prognostic and diagnostic heat flux–based estimates agreed well with the observed Ar/N_2 seasonal cycle, but at other sites, including AMS, MQA and SYO, the observed cycles had later maxima than the modeled cycles. Modeled seasonal amplitudes were larger at some sites, smaller at others compared to observations. Large observational uncertainties have contributed to the ambiguous results of model-data Ar/N_2 comparisons.

[31] Figure 6 shows that subtracting APO_{therm} from observed APO yields a net biological cycle that is smaller in amplitude but similar in phasing to the original APO signal. Depending on which thermal APO signal is subtracted, the observed APO amplitude is reduced by 20–30%, making the thermal correction a relatively small but not negligible

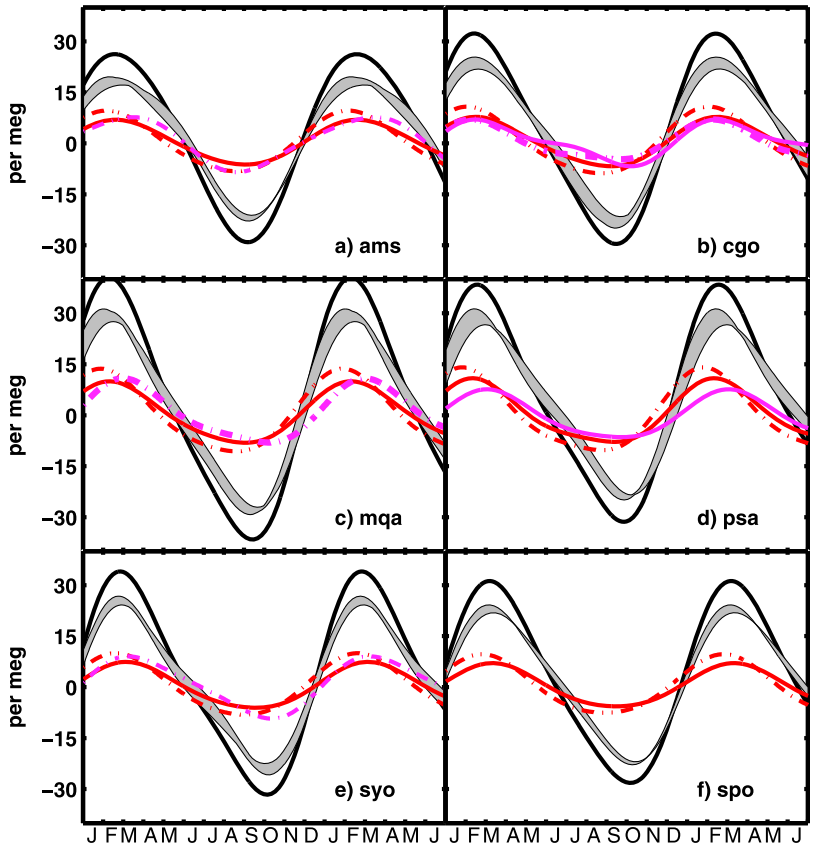

Figure 6. Estimated thermal APO cycles (colored lines) and thermally corrected APO cycles (gray windows) at six stations. Black curves show observed APO cycle. Red curves show results of MATCH simulations forced with thermal O_2 and N_2 fluxes estimated from QS_T/C_p (dash dot lines) or QS_T/C_p with the *Jin et al.* [2007] modifications (solid lines). Magenta curves show thermal APO cycles estimated from SIO (solid) and PU (dash dot) Ar/N_2 data. The gray windows represent the range of thermally corrected APO cycles (i.e., the net biological signal APO_{netbio}) resulting from subtracting all viable thermal APO cycles, both modeled and Ar/N_2-based, from observed APO.

source of uncertainty in our decomposition of the APO cycle. For N_2O, the uncertainty in the thermal cycle has relatively more importance, and this feeds back on our inferred APO_{vent} and APO_{NCP} signals, as discussed below.

3.3. Decomposition of the APO Net Biological Signal

[32] Here, we decompose APO_{netbio} into deep ventilation (APO_{vent}) and net community production (APO_{NCP}) signals using the N_2O-based method (Section 2.7). We restrict this analysis to three sites: CGO, PSA, and SPO, where atmospheric N_2O and CFC-12 data are both available (Table S1). Among these sites, we have the most confidence in our results at CGO and SPO, where high frequency in situ N_2O time series are available and yield consistent mean seasonal cycles that are relatively independent of the range of years over which we analyze the data. In contrast, the flask N_2O measurements at PSA are more interannually variable and probably overestimate the true mean seasonal cycle [*Nevison et al.*, 2011]. At all three sites, we compare our N_2O and APO-based atmospheric signals to independent estimates from our MATCH simulations.

3.3.1. Cape Grim, Tasmania

[33] Our analysis at CGO begins with the decomposition of the atmospheric N_2O seasonal cycle (Figure 7a). We quickly identified the thermal signal as a large source of uncertainty in the analysis and therefore present our results in terms of their sensitivity to three alternative estimates of N_2O_{therm} and APO_{therm} based on 1) SIO Ar/N_2 data, 2) the QS_T/Cp formula and 3) the modified QS_T/Cp formula. The three alternatives lead to a 1.5-month spread in the maximum of the inferred N_2O_{vent} signal, which is determined largely by the phasing of the minimum in N_2O_{therm}. Thermal signal #3, ATM-N_2OTHERM$_{Qmod}$, gives an N_2O_{vent} signal with an early October maximum, which agrees best in phase with two independent estimates based on ocean model N_2O fluxes, ATM-N_2OVENT$_{MIT}$ and ATM-N_2OVENT$_{JG}$ (Figure 7c). Thermal signal #1, $N_2O_{therm,Ar}$, gives a late October/early November peak in N_2O_{vent}, which appears late compared to the independent estimates. The physics of deep ventilation in the Southern Ocean, beginning with the breakdown of the oceanic mixed layer in fall and ending with re-stratification of the surface ocean in spring, also tend to argue against a late October ventilation peak. Thermal signal #2, ATM-N_2OTHERM$_Q$, gives a mid-September N_2O_{vent} maximum, which appears early compared to the ocean model estimates.

[34] The amplitude of N_2O_{vent} inferred from atmospheric data (using the optimal thermal signal ATM-N_2OTHERM$_{Qmod}$)

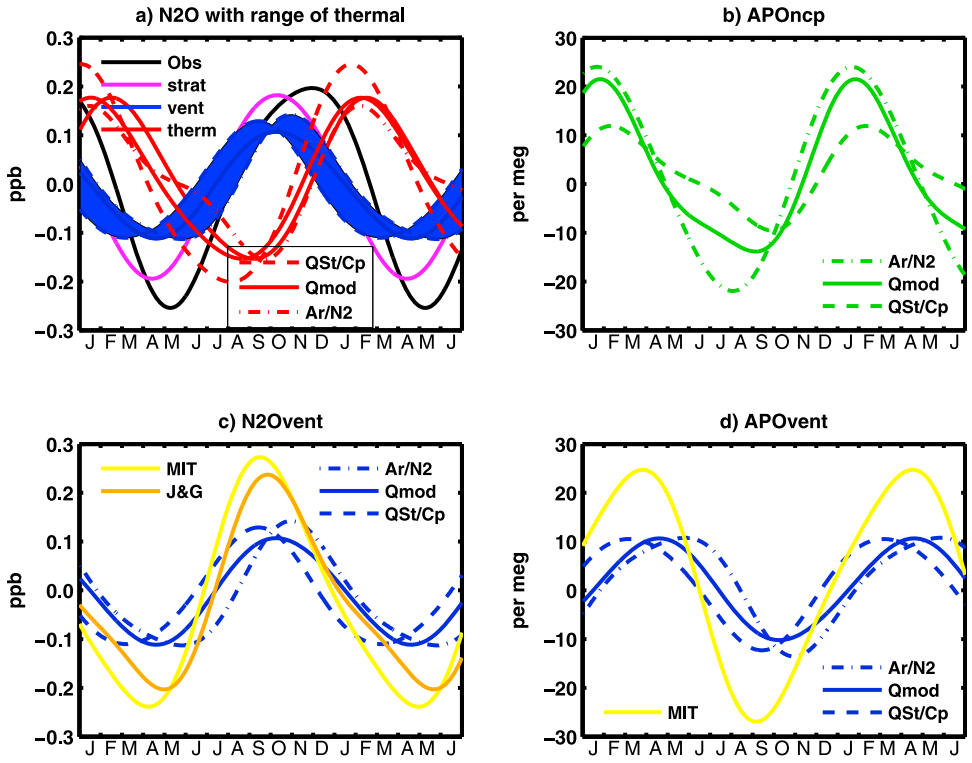

Figure 7. Selected components of the (left) N_2O or (right) APO mean seasonal cycles at Cape Grim, Tasmania, showing sensitivity to choice of thermal signal. (a) Shows all terms in the N_2O cycle, in which observed (black) and stratospheric (magenta) signals are represented as single lines and considered well known. (All calculations use constant CFC-12n scalar of $\alpha = 0.7$ to estimate N_2O_{strat}.) Red lines show range of choices for N_2O_{therm} (dash = QS_T/Cp, solid = modified QS_T/Cp, dash-dot = SIO Ar/N_2-based). Blue envelope shows resulting range of uncertainty in N_2O_{vent}, which is calculated as a residual of the other terms. (b) Range of uncertainty in inferred APO_{NCP} resulting from choice of thermal signal, (c) range of uncertainty in $N2O_{vent}$ resulting from choice of thermal signal, with comparisons to independent estimates from MATCH simulations: yellow = ATM-$N2OVENT_{MIT}$ (reduced by a factor of 2 to keep other curves legible), orange = ATM-$N2OVENT_{JG}$. (d) Range of uncertainty in APO_{vent} resulting from choice of thermal signal, with comparison to independent estimate from ATM-$VENT_{MIT}$ (yellow).

is smaller by a factor of 2 to 4 than that of ATM-N_2OVENT_{JG} and ATM-N_2OVENT_{MIT} (Figure 7c). The N_2O source predicted by the underlying ocean models is 0.9 and 1.8 Tg N/yr, respectively, from the region south of 30°S. This result differs from that of *Nevison et al.* [2005], who found that the inferred N_2O_{vent} signal was generally consistent with *Jin and Gruber*'s [2003] ocean model source. The main difference from our current study is that *Nevison et al.* [2005] assumed a modeled value of N_2O_{therm} that was similar in amplitude to the ATM-$N_2OTHERM_Q$ signal shown here but was shifted 1 month later, which is substantially different than any of the thermal signals tested in the current study. The new results suggest that the Southern Ocean N_2O source may be only on the order of 0.5 Tg N/yr. While smaller than the independent ocean model estimates, this new value is still large compared to recent estimates of the N_2O source from the 30–90° latitude band derived from atmospheric N_2O inversions, which in some configurations predict a near-zero or even negative source [*Hirsch et al.*, 2006; *Huang et al.*, 2008].

[35] Turning to the decomposition of the observed APO seasonal cycle, APO_{vent} can be estimated from N_2O_{vent}, which allows APO_{NCP} to be estimated as a residual using equations (7)–(8) (Figures 7c and 7d). A comparison of APO_{NCP} to independent estimates based on satellite ocean color or the MIT ocean model shows that all estimates are generally consistent in shape and phase (Figure 8a). This agreement was by no means guaranteed at the outset of our study and allows the amplitudes of the independent estimates of NCP to be compared directly for the first time to the APO-based constraint. Figure 8a shows that the smaller of the two satellite-based signals, ATM-NCP_{EP12}, agrees best in amplitude with our best guess estimate of APO_{NCP}, suggesting that an NCP flux of 12 Pg C/yr (1 Pg C/yr south of 50°S) is consistent with APO data. In contrast, the amplitudes of ATM-NCP_{EP17} and ATM-NCP_{MIT} tend to push or exceed the upper limit allowed by the decomposed APO data, suggesting the underlying NCP fluxes are too large. This is true even within the relatively wide range of uncertainty in APO_{NCP}, which derives mainly from the sensitivity of N_2O_{vent}, and thus APO_{vent} and APO_{NCP}, to the choice of thermal signal.

[36] Figure 9 shows the observed APO seasonal cycle partitioned into its component biological signals. Several

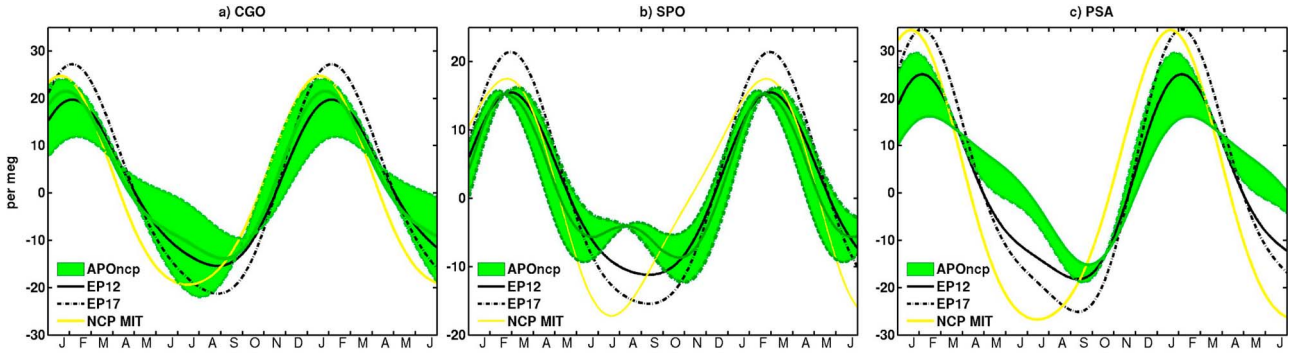

Figure 8. Comparison of APO_{NCP} derived from the N_2O-based method, shown as a green window of uncertainty (see Figures 7, S1, and S3 for details) to independent estimates based on satellite ocean color data, ATM-NCP_{EP12} (solid black) and ATM-NCP_{EP17} (dash-dot black), and an ocean biogeochemistry model, ATM-NCP_{MIT} (yellow). (a) Cape Grim, (b) South Pole, (c) Palmer Station.

alternative views are presented, reflecting the uncertainty discussed above, but the partitioned cycles share some common features. The springtime rise in the APO cycle leading to the summer maximum is dictated mainly by the NCP signal, while the late winter/early spring minimum is governed mainly by the ventilation signal. Our best guess estimate (based largely on its optimal N_2O_{vent} signal), suggests that APO_{NCP} and APO_{vent} do not directly overlap (i.e., are not 6 months out of phase, with opposite sign), as was assumed, e.g., by *Keeling et al.* [1993], but rather are staggered and only partly reinforcing. With only partly reinforcing signals, larger component NCP and ventilation fluxes are needed, compared to the fully reinforcing case, to achieve the same overall APO amplitude.

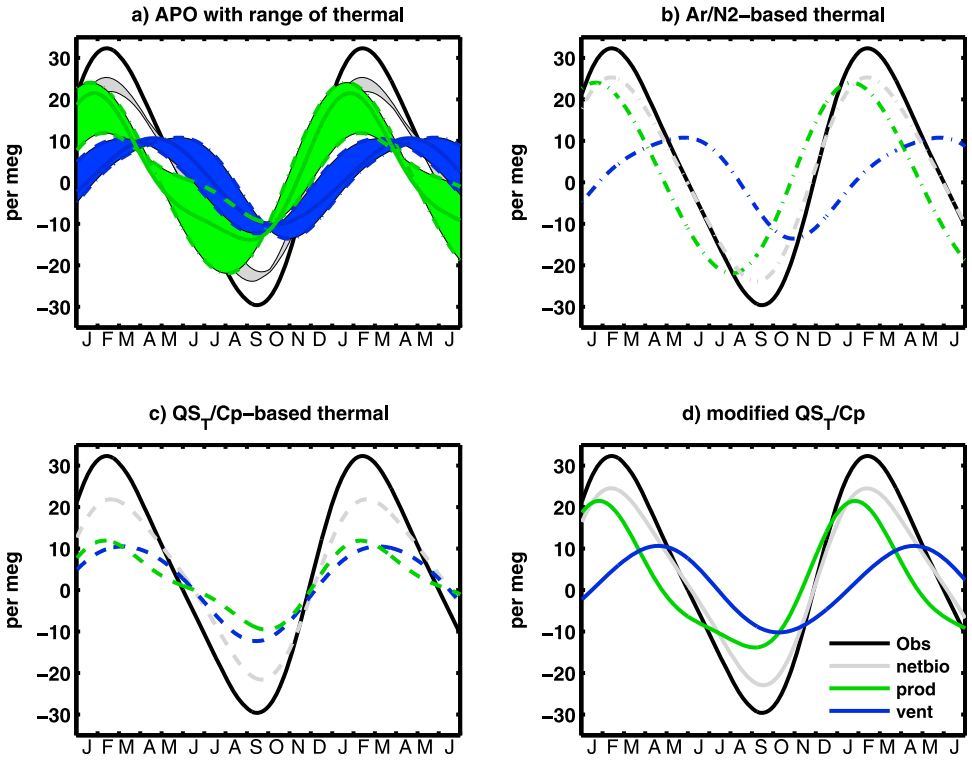

Figure 9. Decomposition of the mean seasonal cycle in APO at Cape Grim, Tasmania, showing sensitivity to choice of thermal signal (see Figure 7 for details of corresponding N_2O cycle). Black = observed, gray = net biological signal (i.e., observed minus thermal correction), green = NCP, blue = ventilation. (a) APO cycle considering 3 different choices of thermal signal (for both APO and N_2O), with envelopes showing ranges of uncertainty. Figures 9b–9d show three alternative representations of the decomposed APO seasonal cycle using the following thermal signals: (b) Ar/N_2-based, (c) QS_T/Cp-based, (d) QS_T/Cp-based signal modified according to *Jin et al.* [2007].

3.3.2. South Pole and Palmer Station

[37] We performed similar decompositions of the APO seasonal cycle using the N_2O-based method at two additional sites, SPO and PSA. The decomposition at SPO focuses on the sensitivity of our results to uncertainty in the N_2O_{strat} term, while the decomposition at PSA, like that at CGO, focuses on the sensitivity to the thermal signal. Details are presented in Text S2. Figure 8 summarizes the results of Section 3.3 by showing that APO_{NCP} is generally consistent at all three sites with the smaller of the two satellite ocean color-based estimates, ATM-NCP_{EP12}, corresponding to an NCP flux of 1 Pg C/yr south of 50°S, and inconsistent with the larger estimate ATM-NCP_{EP17}.

[38] If we assume that the difference in seasonal amplitude between ATM-NCP_{EP12} and ATM-NCP_{EP17} (corresponding to 1.05 and 1.4 Pg C/yr south of 50°S) scales linearly and can be applied to the range in APO_{NCP} shown in Figure 8, we obtain quantitative bounds on NCP of 0.69–1.3, 0.80–1.2 and 0.96–1.1 Pg C/yr using APO data at CGO, PSA and SPO, respectively. PSA and SPO are influenced primarily by processes occurring south of 50°S, whereas CGO is also influenced by more equatorward latitudes [*Garcia and Keeling*, 2001]. The relatively tight constraint at SPO in part reflects the fact that our analysis focuses on the sensitivity of N_2O_{vent} and thus APO_{vent} to stratospheric influences, but does not take into account the larger sensitivity to thermal influences (due to the unavailability of Ar/N_2 data at SPO). We therefore take the larger of the PSA and SPO results, 0.8–1.2 Pg C/yr, as our best quantitative estimate of the constraint on NCP south of 50°S provided by APO. Notably this estimate does not account for additional atmospheric transport model uncertainties associated with the calculation of ATM-NCP_{EP12} and ATM-NCP_{EP17}.

4. Discussion

[39] Both satellite ocean color data and observed seasonal cycles in APO offer a means to estimate net community production and the corresponding air-sea flux of O_2 during the phytoplankton growing season. APO data, which are measured at high precision, are used here to constrain the satellite-based estimates, which provide detailed spatial and temporal coverage but are uncertain in magnitude, especially for higher order products like NPP and export production. However, a caveat on our study is that APO is measured in units of per meg and thus provides a measure of the pulse of O_2 diluted into a given volume of air, rather than an absolute measure of the pulse of O_2. Atmospheric transport models (ATMs) are the best available tool for estimating the atmospheric dilution of a surface O_2 pulse, but such models unavoidably introduce uncertainty in the comparison of surface air-sea fluxes to atmospheric data [*Naegler et al.*, 2007]. This problem is especially pronounced at sites such as Palmer Station, Antarctica, featured in this study, or Northern Hemisphere sites like Cold Bay, Alaska [*Gruber et al.*, 2001; *Battle et al.*, 2006], where the air-sea O_2 flux is concentrated over a relatively short span of months and interacts with seasonal covariance in boundary layer thickness and other transport and mixing properties. In summer, the marine boundary layer is relatively shallow and tends to trap O_2 fluxes associated with NCP near the surface, but the extent of this trapping is ATM sensitive. In winter, the boundary layer is thicker due to warming of the atmosphere by convective heating from the ocean, such that the oceanic ventilation signal is diluted into a larger atmospheric volume, but the extent of dilution is also ATM sensitive [*Gruber et al.*, 2001; *Blaine*, 2005; *Nevison et al.*, 2008].

[40] Here, we have reported results using a single ATM, MATCH:NCEP, to translate two satellite-based NCP estimates into APO signals. By convolving these results with APO observations at two Southern Ocean monitoring sites, we estimate an NCP flux of 0.8–1.2 Pg C/yr south of 50°S. Our estimate is consistent with the independent estimate of new production south of 50°S of 1.1 ± 0.2 Pg C/yr based on wind-driven upwelling rates and observed nitrate at depth [*Pollard et al.*, 2006]. However, we must acknowledge that the APO Transcom experiment [*Blaine*, 2005] suggested that MATCH:NCEP yields relatively large seasonal amplitudes compared to some other ATMs when forced with the same surface O_2 fluxes. Thus, for some ATMs, it is possible that the larger satellite-based estimate, ATM-NCP_{EP17}, would be more compatible with the APO-based constraint and thus that a larger NCP flux south of 50°S would be indicated. To tighten the constraint that APO seasonal cycles can provide on satellite ocean color data, ATM uncertainty must be reduced.

[41] On a related note, Ar/N_2 data in principle provide the best basis for estimating the N_2O_{therm} and APO_{therm} signals used in this study because Ar/N_2 is a direct atmospheric measurement that avoids the need for the mediation of an ATM. It is therefore perplexing that the use of $N_2O_{therm,Ar}$ at both CGO and PSA leads to an N_2O_{vent} signal whose maximum appears to occur unreasonably late in the spring (see Section 3.3.1, Text S2). This puzzling result may reflect uncertainties in Ar/N_2 data, as discussed in Section 3.2, but it also raises questions about a possible missing signal in our decomposition of the observed N_2O seasonal cycle. Text S3 investigates the possibility of a missing terrestrial N_2O signal and concludes that such a signal cannot be ruled out, but will tend to shift the inferred N_2O_{vent} maximum even later in the spring, thus exacerbating the problem. Alternatively, it is possible that there is a component of the N_2O flux associated with nitrification at the base of the euphotic zone that correlates more strongly to O_2 production than to deep ventilation [*Charpentier et al.*, 2007; *Yool et al.*, 2007]. In addition, stations located near Antarctica may be influenced by a pulse of upwelled N_2O that has accumulated beneath winter sea ice and is abruptly released to the atmosphere during spring/summer ice retreat [*Rees et al.*, 1997].

[42] We expect that aircraft campaigns to measure altitude profiles of important trace gases over large spatial domains will help reduce many of the uncertainties discussed above. The HIPPO campaign in particular will provide an extensive, seasonally resolved data set of APO and other trace gases like N_2O, CFC-12 and Ar/N_2, which will help quantify the extent to which surface emissions are trapped in the boundary layer, thereby providing more rigorous constraints on ATMs than are currently available [*Stephens et al.*, 2007; *Wofsy et al.*, 2011]. HIPPO will also permit comparisons of concurrent atmospheric N_2O and APO variability over a full seasonal cycle in the Southern Ocean region and will provide improved constraints on stratospheric contributions to tropospheric variability.

[43] Even after ATM and other uncertainties pertaining to the APO versus N_2O relationship are narrowed, an important remaining uncertainty is the conversion of satellite ocean color data into F_{O2}, the air-sea O_2 flux. From a conceptual standpoint, this conversion is problematic because it attempts to relate satellite-derived export production at 100 m to a surface flux. We have addressed this problem by arguing that 1) satellite ocean color data are fundamentally a near-surface measurement, 2) the phasing and magnitude of EP, as derived from ocean color, are similar to those of NCP, and 3) NCP is logically linked to F_{O2}. These arguments are consistent with the assumptions made in deriving the model by *Laws et al.* [2000] and *Laws* [2004] for estimating the *f* ratio, i.e., that EP balances new production. The good agreement between APO_{NCP} and ATM-NCP_{EP12} derived here supports these assumptions, as does the agreement in shape and phase between APO_{NCP} and ATM-NCP_{MIT} (Figure 8). One also can perform an independent, internal check using the MIT ocean model, based on the comparison of F_{O2} associated with NCP, converted to carbon units, and the model EP, calculated by multiplying the POC concentration at the base of the mixed layer by the prescribed (constant) sinking velocity. These two fluxes are roughly in balance at 16.7 and 15.7 Pg C/yr, respectively, providing support for the simple assumptions of our study. There are, however, some regional and phase imbalances between MIT model NCP and EP that tend to undermine the equivalence. In addition, the version of the MIT model used here has relatively coarse vertical resolution, with positive NCP more or less confined to the surface layer, which may affect the relationships among F_{O2}, NCP and EP. Results from other 3-dimensional ocean biogeochemistry models, with higher vertical resolution and O_2 tracers decomposed as outlined in Section 2.4, would be valuable for evaluating the robustness of the relationships between EP, NCP and F_{O2} presented here.

5. Conclusions

[44] Three independent approaches, based on atmospheric APO and N_2O observations, satellite ocean color data, and a 3-dimensional ocean biogeochemistry model, provide a consistent picture of the partitioning of biological air-sea O_2 fluxes in the Southern Ocean and their corresponding atmospheric signals. Among the most important results of our study are: 1) Chl-a and associated NPP fluxes derived from satellite ocean color data historically have been underestimated in the Southern Ocean. Traditional models [*Laws et al.*, 2000; *Laws*, 2004] using upward-revised NPP inputs tend to overestimate *f* ratios and thus EP and NCP, according to APO-based constraints. Our study suggests that NCP south of 50°S is likely about 1 Pg C yr^{-1}, with an average *f* ratio of 0.33. 2) O_2 fluxes associated with NCP occur primarily in spring/summer in the mid to high latitude Southern Ocean, while O_2 fluxes associated with deep ventilation occur primarily in winter. Although the underlying air-sea fluxes are seasonally distinct, their corresponding atmospheric signals overlap and are affected further by covariance with atmospheric transport and boundary layer thickness. 3) The seasonal N_2O flux from the Southern Ocean (30–90°S) is estimated here at ~0.5 Tg N/yr. This flux is smaller than previously reported estimates based on ocean models and dissolved N_2O data, but larger than estimates from recent atmospheric N_2O inversions.

[45] Our study identifies some important future steps for reducing current uncertainties and thereby improving the quantitative constraints that APO data can provide on carbon and oxygen fluxes derived from satellite ocean color data. Foremost among these is the need for better constraints on atmospheric transport models, which are necessary for translating satellite ocean color data into atmospheric APO signals. We expect substantial progress in this arena thanks to recent aircraft campaigns to measure altitude profiles of APO, N_2O, and other important trace gases and their seasonal and spatial variability. In addition to refinements of ATMs, efforts are needed to better identify the relationships among F_{O2}, NCP and EP, using e.g., high-resolution 3-D ocean biogeochemistry models. Finally, the thermal signals used to correct observed seasonal cycles in atmospheric data to infer biological signals are a source of uncertainty that is larger than previously appreciated, especially for relatively soluble gases like N_2O. Further work is needed to reconcile the thermal signals derived from Ar/N_2 data with signals derived from ocean models and ocean heat flux data.

[46] **Acknowledgments.** The authors gratefully acknowledge Michael Bender and Robert Mika for providing APO and Ar/N_2 data, and Paul Fraser, Paul Krummel and Paul Steele, Ed Dlugokencky, and Geoff Dutton, Jim Elkins and Brad Hall for providing N_2O and CFC-12 data from Cape Grim, Palmer Station, and the South Pole, respectively. We also thank Stephanie Dutkiewicz, Parv Suntharalingam and Xin Jin for ocean biogeochemistry modeling assistance and output. We thank two anonymous reviewers for helpful comments and acknowledge support from NASA Ocean Biology and Biogeochemistry grant NNX08AB48G.

References

Anderson, L. (1995), On the hydrogen and oxygen content of marine phytoplankton, *Deep Sea Res., Part I*, *42*, 1675–1680, doi:10.1016/0967-0637(95)00072-E.

Antoine, D., J.-M. André, and A. Morel (1996), Oceanic primary production: 2. Estimation at global scale from satellite (Coastal Zone Color Scanner) chlorophyll, *Global Biogeochem. Cycles*, *10*(1), 57–69, doi:10.1029/95GB02832.

Balkanski, Y., P. Monfray, M. Battle, and M. Heimann (1999), Ocean primary production derived from satellite data: An evaluation with atmospheric oxygen measurements, *Global Biogeochem. Cycles*, *13*(2), 257–271, doi:10.1029/98GB02312.

Battle, M., M. Bender, M. B. Hendricks, D. T. Ho, R. Mika, G. McKinley, S.-M. Fan, T. Blaine, and R. F. Keeling (2003), Measurements and models of the atmospheric Ar/N_2 ratio, *Geophys. Res. Lett.*, *30*(15), 1786, doi:10.1029/2003GL017411.

Battle, M., et al. (2006), Atmospheric potential oxygen: New observations and their implications for some atmospheric and oceanic models, *Global Biogeochem. Cycles*, *20*, GB1010, doi:10.1029/2005GB002534.

Behrenfeld, M. J., and P. G. Falkowski (1997), Photosynthetic rates derived from satellite-based chlorophyll concentration, *Limnol. Oceanogr.*, *42*(1), 1–20, doi:10.4319/lo.1997.42.1.0001.

Bender, M., J. T. Ellis, P. P. Tans, R. J. Francey, and D. Lowe (1996), Variability in the O_2/N_2 ratio of Southern Hemisphere air, 1991–1994: Implications for the carbon cycle, *Global Biogeochem. Cycles*, *10*(1), 9–21, doi:10.1029/95GB03295.

Bender, M., D. Ho, M. B. Hendricks, R. Mika, M. O. Battle, P. Tans, T. J. Conway, P. B. Sturtevant, and N. Cassar (2005), Atmospheric O_2/N_2 changes, 1993–2002: Implications for the partitioning of fossil fuel CO_2 sequestration, *Global Biogeochem. Cycles*, *19*, GB4017, doi:10.1029/2004GB002410.

Blaine, T. W. (2005), Continuous measurements of atmospheric Ar/N_2 as a tracer of air-sea heat flux: Models, methods, and data, PhD dissertation, 225 pp., Univ. of Calif., San Diego, La Jolla.

Butler, J. H., J. W. Elkins, T. M. Thompson, and K. B. Egan (1989), Tropospheric and dissolved N_2O of the West Pacific and East Indian Oceans during the El Niño Southern Oscillation event of 1987, *J. Geophys. Res.*, *94*, 14,865–14,877, doi:10.1029/JD094iD12p14865.

Caldeira, K., and P. B. Duffy (2000), The role of the Southern Ocean in uptake and storage of anthropogenic carbon dioxide, *Science*, *287*(5453), 620–622, doi:10.1126/science.287.5453.620.

Carr, M.-E., et al. (2006), A comparison of global estimates of marine primary production from ocean color, *Deep Sea Res., Part II*, *53*, 741–770, doi:10.1016/j.dsr2.2006.01.028.

Cassar, N., G. A. McKinley, M. L. Bender, R. Mika, and M. Battle (2008), An improved comparison of atmospheric Ar/N_2 time series and paired ocean-atmosphere model predictions, *J. Geophys. Res.*, *113*, D21122, doi:10.1029/2008JD009817.

Charpentier, J., L. Farias, N. Yoshida, N. Boontanon, and P. Raimbault (2007), Nitrous oxide distribution and its origin in the central and eastern South Pacific Subtropical Gyre, *Biogeosciences Discuss.*, *4*, 1673–1702, doi:10.5194/bgd-4-1673-2007.

Cohen, Y., and L. I. Gordon (1978), Nitrous oxide in the oxygen minimum of the eastern tropical North Pacific: Evidence for its consumption during denitrification and possible mechanisms for its production, *Deep Sea Res.*, *25*, 509–524, doi:10.1016/0146-6291(78)90640-9.

Dunne, J. P., R. A. Armstrong, A. Gnanadesikan, and J. L. Sarmiento (2005), Empirical and mechanistic models for the particle export ratio, *Global Biogeochem. Cycles*, *19*, GB4026, doi:10.1029/2004GB002390.

Dutkiewicz, S., M. J. Follows, and P. Parekh (2005), Interactions of the iron and phosphorus cycles: A three-dimensional model study, *Global Biogeochem. Cycles*, *19*, GB1021, doi:10.1029/2004GB002342.

Eppley, R. W., and B. J. Peterson (1979), Particulate organic matter flux and planktonic new production in the deep ocean, *Nature*, *282*, 677–680, doi:10.1038/282677a0.

Friedrichs, M. A. M., et al. (2009), Assessing the uncertainties of model estimates of primary productivity in the tropical Pacific Ocean, *J. Mar. Syst.*, *76*(1–2), 113–133, doi:10.1016/j.jmarsys.2008.05.010.

Garcia, H. E., and R. F. Keeling (2001), On the global oxygen anomaly and air-sea flux, *J. Geophys. Res.*, *106*, 31,155–31,166, doi:10.1029/1999JC000200.

Gruber, N., and J. L. Sarmiento (2002), Large-scale biogeochemical-physical interactions in elemental cycles, in *The Sea*, vol. 12, edited by A. R. Robinson, J. J. McCarthy, and B. J. Rothschild, pp. 337–399, John Wiley, New York.

Gruber, N., M. Gloor, S.-M. Fan, and J. L. Sarmiento (2001), Air-sea flux of oxygen estimated from bulk data: Implications for the marine and atmospheric oxygen cycles, *Global Biogeochem. Cycles*, *15*(4), 783–803, doi:10.1029/2000GB001302.

Hallberg, R., and A. Gnanadesikan (2006), The role of eddies in determining the structure and response of the wind-driven Southern Hemisphere overturning: Results from the modeling eddies in the Southern Ocean (MESO) project, *J. Phys. Oceanogr.*, *36*, 2232–2252, doi:10.1175/JPO2980.1.

Hirsch, A. I., A. M. Michalak, L. M. Bruhwiler, W. Peters, E. J. Dlugokencky, and P. P. Tans (2006), Inverse modeling estimates of the global nitrous oxide surface flux from 1998–2001, *Global Biogeochem. Cycles*, *20*, GB1008, doi:10.1029/2004GB002443.

Horrigan, S. G., A. F. Carlucci, and P. M. Williams (1981), Light inhibition of nitrification in sea-surface films, *J. Mar. Res.*, *39*, 557–565.

Huang, J., et al. (2008), Estimation of regional emissions of nitrous oxide from 1997 to 2005 using multinetwork measurements, a chemical transport model, and an inverse method, *J. Geophys. Res.*, *113*, D17313, doi:10.1029/2007JD009381.

Ito, T., P. Parekh, S. Dutkiewicz, and M. J. Follows (2005), The Antarctic Circumpolar Productivity Belt, *Geophys. Res. Lett.*, *32*, L13604, doi:10.1029/2005GL023021.

Jin, X., and N. Gruber (2003), Offsetting the radiative benefit of ocean iron fertilization by enhancing N_2O emissions, *Geophys. Res. Lett.*, *30*(24), 2249, doi:10.1029/2003GL018458.

Jin, X., R. G. Najjar, F. Louanchi, and S. C. Doney (2007), A modeling study of the seasonal oxygen budget of the global ocean, *J. Geophys. Res.*, *112*, C05017, doi:10.1029/2006JC003731.

Kahru, M., and B. G. Mitchell (2010), Blending of ocean color algorithms applied to the Southern Ocean, *Remote Sens. Lett.*, *1*, 119–124, doi:10.1080/01431160903547940.

Kalnay, E., et al. (1996), The NMC/NCAR 40-year reanalysis project, *Bull. Am. Meteorol. Soc.*, *77*, 437–471, doi:10.1175/1520-0477(1996)077<0437:TNYRP>2.0.CO;2.

Keeling, R. F., and S. R. Shertz (1992), Seasonal and interannual variations in atmospheric oxygen and implications for the global carbon cycle, *Nature*, *358*, 723–727, doi:10.1038/358723a0.

Keeling, R. F., R. P. Najjar, M. L. Bender, and P. P. Tans (1993), What atmospheric oxygen measurements can tell us about the global carbon cycle, *Global Biogeochem. Cycles*, *7*, 37–67, doi:10.1029/92GB02733.

Keeling, R. F., S. C. Piper, and M. Heimann (1996), Global and hemispheric CO_2 sinks deduced from changes in atmospheric O_2 concentration, *Nature*, *381*, 218–221, doi:10.1038/381218a0.

Keeling, R. F., B. B. Stephens, R. G. Najjar, S. C. Doney, D. Archer, and M. Heimann (1998), Seasonal variations in the atmospheric O_2/N_2 ratio in relation to the kinetics of air-sea gas exchange, *Global Biogeochem. Cycles*, *12*, 141–163, doi:10.1029/97GB02339.

Keeling, R. F., T. Blaine, B. Paplawsky, L. Katz, C. Atwood, and T. Brockwell (2004), Measurement of changes in atmospheric Ar/N_2 ratio using a rapid-switching, single-capillary mass spectrometer system, *Tellus, Ser. B*, *56*, 322–338, doi:10.1111/j.1600-0889.2004.00117.x.

Khatiwala, S., F. Primeau, and T. Hall (2009), Reconstruction of the history of anthropogenic CO_2 concentrations in the ocean, *Nature*, *462*, 346–349, doi:10.1038/nature08526.

Laws, E. A. (1991), Photosynthetic quotients, new production and net community production in the open ocean, *Deep Sea Res., Part A*, *38*, 143–167.

Laws, E. A. (2004), Export flux and stability as regulators of community composition in pelagic marine biological communities: Implications for regime shifts, *Prog. Oceanogr.*, *60*(2–4), 343–354, doi:10.1016/j.pocean.2004.02.015.

Laws, E. A., P. G. Falkowski, W. O. Smith Jr., H. W. Ducklow, and J. J. McCarthy (2000), Temperature effects on export production in the open ocean, *Global Biogeochem. Cycles*, *14*(4), 1231–1246, doi:10.1029/1999GB001229.

Le Quéré, C., et al. (2008), Saturation of the Southern Ocean CO_2 sink due to recent climate change, *Science*, *316*, 1735–1738.

Longhurst, A., S. Sathyendranath, T. Platt, and C. Caverhill (1995), An estimate of global primary production in the ocean from satellite radiometer data, *J. Plankton Res.*, *17*(6), 1245–1271, doi:10.1093/plankt/17.6.1245.

Lovenduski, N. S., N. Gruber, S. C. Doney, and I. D. Lima (2007), Enhanced CO_2 outgassing in the Southern Ocean from a positive phase of the Southern Annular Mode, *Global Biogeochem. Cycles*, *21*, GB2026, doi:10.1029/2006GB002900.

Lueker, T. J., S. J. Walker, M. K. Vollmer, R. F. Keeling, C. D. Nevison, R. F. Weiss, and H. E. Garcia (2003), Coastal upwelling air-sea fluxes revealed in atmospheric observations of O_2/N_2, CO_2 and N_2O, *Geophys. Res. Lett.*, *30*(6), 1292, doi:10.1029/2002GL016615.

Mahowald, N. M., P. J. Rasch, B. E. Eaton, S. Whittlestone, and R. G. Prinn (1997), Transport of ^{222}radon to the remote troposphere using the Model of Atmospheric Transport and Chemistry and assimilated winds from ECMWF and the National Center for Environmental Prediction/NCAR, *J. Geophys. Res.*, *102*, 28,139–28,151, doi:10.1029/97JD02084.

Manning, A. C., and R. F. Keeling (2006), Global oceanic and land biotic carbon sinks from the Scripps atmospheric oxygen flask sampling network, *Tellus, Ser. B*, *58*, 95–116, doi:10.1111/j.1600-0889.2006.00175.x.

Marshall, J., C. Hill, L. Perelman, and A. Adcroft (1997a), Hydrostatic, quasi-hydrostatic and nonhydrostatic ocean modeling, *J. Geophys. Res.*, *102*, 5733–5752, doi:10.1029/96JC02776.

Marshall, J., A. Adcroft, C. Hill, L. Perelman, and C. Heisey (1997b), A finite-volume, incompressible Navier-Stokes model for the studies of the ocean on parallel computers, *J. Geophys. Res.*, *102*, 5753–5766, doi:10.1029/96JC02775.

Mitchell, B. G. (1992), Predictive bio-optical relationships for polar oceans and marginal ice zones, *J. Mar. Syst.*, *3*, 92–105.

Mitchell, B. G., and O. Holm-Hansen (1991), Bio-optical properties of Antarctic Peninsula waters: Differentiation from temperate ocean models, *Deep Sea Res., Part A*, *38*, 1009–1028, doi:10.1016/0198-0149(91)90094-V.

Mitchell, B. G., and M. Kahru (2009), Bio-optical algorithms for ADEOS-2 GLI, *J. Remote Sens. Soc. Jpn.*, *29*(1), 80–85.

Naegler, T., P. Ciais, J. Orr, O. Aumont, and C. Roedenbeck (2007), On evaluating ocean models with atmospheric potential oxygen, *Tellus*, *59B*, 138–156.

Najjar, R. G., and R. F. Keeling (2000), Mean annual cycle of the air-sea oxygen flux: A global view, *Global Biogeochem. Cycles*, *14*(2), 573–584, doi:10.1029/1999GB900086.

Nevison, C., J. H. Butler, and J. W. Elkins (2003), Global distribution of N_2O and the ΔN_2O-AOU yield in the subsurface ocean, *Global Biogeochem. Cycles*, *17*(4), 1119, doi:10.1029/2003GB002068.

Nevison, C. D., R. F. Keeling, R. F. Weiss, B. N. Popp, X. Jin, P. J. Fraser, L. W. Porter, and P. G. Hess (2005), Southern Ocean ventilation inferred from seasonal cycles of atmospheric N_2O and O_2/N_2 at Cape Grim, Tasmania, *Tellus, Ser. B*, *57*, 218–229.

Nevison, C. D., N. M. Mahowald, S. C. Doney, I. D. Lima, and N. Cassar (2008), Impact of variable air-sea O_2 and CO_2 fluxes on atmospheric potential oxygen (APO) and land-ocean carbon sink partitioning, *Biogeosciences*, *5*, 875–889, doi:10.5194/bg-5-875-2008.

Nevison, C. D., et al. (2011), Exploring causes of interannual variability in the seasonal cycles of tropospheric nitrous oxide, *Atmos. Chem. Phys.*, *11*, 3713–3730, doi:10.5194/acp-11-3713-2011.

Pollard, R., P. Tréguer, and J. Read (2006), Quantifying nutrient supply to the Southern Ocean, *J. Geophys. Res.*, *111*, C05011, doi:10.1029/2005JC003076.

Rasch, P. J., N. M. Mahowald, and B. E. Eaton (1997), Representations of transport, convection, and the hydrologic cycle in chemical transport models: Implications for the modeling of short-lived and soluble species, *J. Geophys. Res.*, *102*(D23), 28,127–28,138, doi:10.1029/97JD02087.

Rees, A. P., N. J. P. Owens, and R. C. Upstill-Goddard (1997), Nitrous oxide in the Bellingshausen Sea and Drake Passage, *J. Geophys. Res.*, *102*, 3383–3391, doi:10.1029/96JC03350.

Saba, V. S., et al. (2010), An evaluation of ocean color model estimates of marine primary productivity in coastal and pelagic regions across the globe, *Biogeosciences Discuss.*, *7*(5), 6749–6788, doi:10.5194/bgd-7-6749-2010.

Schlitzer, R. (2002), Carbon export fluxes in the Southern Ocean: Results from inverse modeling and comparison with satellite-based estimates, *Deep Sea Res., Part II*, *49*, 1623–1644, doi:10.1016/S0967-0645(02)00004-8.

Stephens, B. B., R. F. Keeling, M. Heimann, K. D. Six, R. Murnane, and K. Caldeira (1998), Testing global ocean carbon cycle models using measurements of atmospheric O_2 and CO_2 concentration, *Global Biogeochem. Cycles*, *12*, 213–230, doi:10.1029/97GB03500.

Stephens, B. B., et al. (2007), Weak northern and strong tropical land carbon uptake from vertical profiles of atmospheric CO_2, *Science*, *316*, 1732–1735, doi:10.1126/science.1137004.

Suntharalingam, P., and J. L. Sarmiento (2000), Factors governing the oceanic nitrous oxide distribution: Simulations with an ocean general circulation model, *Global Biogeochem. Cycles*, *14*, 429–454, doi:10.1029/1999GB900032.

Thoning, K. W., P. P. Tans, and W. D. Komhyr (1989), Atmospheric carbon dioxide at Mauna Loa Observatory: 2. Analysis of the NOAA GMCC data, 1974–1985, *J. Geophys. Res.*, *94*, 8549–8565, doi:10.1029/JD094iD06p08549.

Toggweiler, J. R., R. Murnane, S. Carson, A. Gnanadesikan, and J. L. Sarmiento (2003), Representation of the carbon cycle in box models and GCMs, 2. Organic pump, *Global Biogeochem. Cycles*, *17*(1), 1027, doi:10.1029/2001GB001841.

Tohjima, Y., H. Mukai, Y. Nojiri, H. Yamagishi, and T. Machida (2008), Atmospheric O_2/N_2 measurements at two Japanese sites: Estimation of global oceanic and land biotic carbon sinks and analysis of the variations in atmospheric potential oxygen (APO), *Tellus, Ser. B.*, *60*, 213–225.

Uitz, J., H. Claustre, B. Gentili, and D. Stramski (2010), Phytoplankton class-specific primary production in the world's oceans: Seasonal and interannual variability from satellite observations, *Global Biogeochem. Cycles*, *24*, GB3016, doi:10.1029/2009GB003680.

Weiss, R. F., and B. A. Price (1980), Nitrous oxide solubility in water and seawater, *Mar. Chem.*, *8*, 347–359.

Wetzel, P., A. Winguth, and E. Maier-Reimer (2005), Sea-to-air CO_2 flux from 1948 to 2003: A model study, *Global Biogeochem. Cycles*, *19*, GB2005, doi:10.1029/2004GB002339.

Wofsy, S. C., HIPPO Science Team and Cooperating Modellers and Satellite Teams (2011), HIAPER Pole-to-Pole Observations (HIPPO): Fine grained, global scale measurements for determining rates for transport, surface emissions, and removal of climatically important atmospheric gases and aerosols, *Philos. Trans. R. Soc. A*, *369*(1943), 2073–2086, doi:10.1098/rsta.2010.0313.

Yool, A., A. P. Martin, C. Fernandez, and D. R. Clark (2007), The significance of nitrification for oceanic new production, *Nature*, *447*, 999–1002, doi:10.1038/nature05885.

Yoshinari, T. (1976), Nitrous oxide in the sea, *Mar. Chem.*, *4*, 189–202, doi:10.1016/0304-4203(76)90007-4.

N. Cassar, Division of Earth and Ocean Sciences, Nicholas School of the Environment, Duke University, Durham, NC 27708, USA.

M. Kahru, R. F. Keeling, B. G. Mitchell, and M. Manizza, Scripps Institution of Oceanography, University of California, San Diego, 9500 Gilman Dr., La Jolla, CA 92093, USA.

C. D. Nevison, INSTAAR, University of Colorado at Boulder, Campus Box 450, Boulder, CO 80309-0450, USA. (nevison@colorado.edu)